Spatial resolution of time-reversal mirrors in two-dimensional and three-dimensional free space environments

Ifanila Rakotoarisoa, David Marx, Christian Prax, Vincent Valeau

Spatial resolution of time-reversal mirrors in two-dimensional and three-dimensional free space environments

I. Rakotoarisoa, D. Marx, C. Prax and V. Valeau

Institut Pprime - D2 - Branche FTC, Université de Poitiers-ENSMA-CNRS, 6, rue Marcel Doré, 86022 Poitiers, France
ifanila.rakotoarisoa@univ-poitiers.fr

Time-reversal can be used to locate unknown acoustics sources in a medium at rest or in a flow. This method is based on the time-reversal invariance of the wave propagation equation. A series of time-reversal simulations has been performed with a "mirror" in a two-dimensional free space environment. The waves propagation is simulated by solving the linearized Euler's equations. The results permit to characterize the time-reversal method in terms of spatial resolution and localisation error by analyzing the focal spot width for each simulation. In this paper, mathematical expressions of the time-reversed pressure and approached formulas for the resolution are derived following the diffraction theory and the phase conjugation in two and three-dimensional cases. Numerical and theoretical results are then compared. The focal spot width is then fully determined by two ratios involving three parameters : the array-source distance,the array length and the wavelength.

1 Introduction

The continuous increase in air, railway and car transports in the last three decades has led to a strong development of imaging and array processing methods such like *beam-forming* and *holography* to identify sound sources responsible for environmental noise. In the late nineties, Mathias Fink et al. [6, 7] have developed a sound source localization method based on the Time-Reversal (TR) technique. It relies on the invariance of wave equation when time is reversed ($t \rightarrow -t$). This property is used to back-propagate waves recorded by a closed or open array of sensors so that the wavefronts focus on the source position. Time-reversal is an extension of a former method called phase conjugation for non-monochromatic sources [7]. These two techniques has been developed for applications in medecine (ultrasonics field), geophysics, underwater acoustics,etc. One of the numerous interests in these methods is that phase-compensation between each sensor is naturally carried out unlike *beam-forming*.

However the TR technique has been rarely applied to aeroacoustics. In this case, due to the presence of a flow, the convected wave equation needs to be used. In order to achieve the Time-Reversal technique, the flow has to be reversed since the Green's function adapted to this configuration is no longer reciprocal. Recently, Deneuve et al. [12] have established the possibility of locating aeroacoustic sources by solving the Euler equations. The technique has also been applied experimentally by Padois et al. [9, 11]: after recording experimental data with a microphone array, the Linear Euler Equations (LEE) were solved numerically to achieve the time-reversed simulation allowing the localization of the noise source. In order to get a better understanding of the potentiality of the technique in the context of flow-noise applications, the objective of this study is to assess the geometrical configurations favorable to an optimal resolution and localization, and the effect of the flow on the resolution. Resolution is indeed a crucial accuracy criteria that evaluates the separation power of any imaging technique.

In section 2, a phase-conjugation model is proposed to assess the resolution of the technique in a theoretical way, while the numerical model is presented in section 3. The results in terms of localization error and resolution are then presented in section 4, before some concluding remarks (section 5).

2 Theoretical model and definitions

2.1 Time-reversal and phase conjugation

The Time-Reversal (TR) method requires two steps to be performed (Figure 1): a recording step and a re-emission

step. Firstly, the acoustic signal generated by an unknown source is recorded by an array of transducers within a period T. The received signal is then re-emitted in backward time (virtually or with an array of transducers) starting with the last recording. In other words, the signal is time-reversed, like a backward-played film. As a result, the wavefronts are gradually reconstructed and finally focused on the initial source position. This operation is mathematically validated
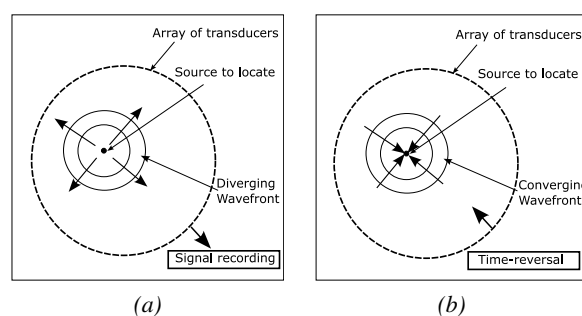

Figure 1: *(a) First step of time-reversal: recording (b) Second step of time-reversal: re-emission*

by the time-reversal invariance of the propagation equation [7] in the case of a non-lossy medium at rest. In the case of a one-dimensional uniform flow $\mathbf{u_0}$, the propagation equation for the pressure fluctuation p' is:

$$(\frac{\partial}{\partial t} + \mathbf{u_0} \cdot \nabla)^2 p' - c_0^2 \nabla^2 p' = 0, \qquad (1)$$

where c_0 is the celerity of sound. With this equation, time-reversal is carried out by replacing t by $T - t$ and $\mathbf{u_0}$ by $-\mathbf{u_0}$. Time invariance is allowed by the second-order derivatives with respect to time.

Two kinds of arrays can be used to record the signal in the first step of time-reversal: a array enclosing the source, also called *cavity*, as shown in Figure 1 or an open array, also called *time-reversal mirror* (TRM). The time-reversal cavity is the optimal solution to get all the information necessary to locate the source [7]. However, this kind of array cannot be used for a periodic source. Indeed, the energy conservation imposes that during the time-reversal the converging wave is followed by a diverging wave [8]. Therefore, the superimposition of converging and diverging waves creates an interference phenomenon. That is why detecting a periodic-source position with a cavity is difficult. Moreover, a closed array would be very expensive in a real experiment since a large number of transducers is required (increasing with the source frequency to respect the Shannon criteria).In order to avoid those issues and get closer to real conditions, the study is restricted to a time-reversal mirror (linear array of transducers). The diverging wave will still exist but it will not interfere with the converging wave generated only by one open array.

Mathematically, in the case of monochromatic sources, time-reversal is equivalent to phase conjugation since the temporal Fourier transform of a time-reversed signal is the conjugate of this signal [7]. In this paper, the phase conjugation theory is used to describe the acoustic pressure field first in a medium at rest, and then in a medium with a one-dimensional uniform flow parallel to the TRM. The propagation environment is free.

2.2 Models for phase conjugated field

Here, the phase-conjugated field produced by a Time-Reversal Mirror in the case of a point-like harmonic monopolar source is investigated. The medium of propagation is two-dimensional and free.

Medium at rest

In first approximation, the TRM can be compared to a continuum of monopolar sources that re-emits in a reversed way the signal received from the unknown source. In terms of phase conjugation, the mirror conjugates the received Fourier transform of the signal. The resulting field for a continuous array is [2]:

$$P_{pc}(\mathbf{r}, \omega) = \int_{TRM} G_{0,\omega}^*(\mathbf{r_i}, \mathbf{r_0}) \cdot G_{0,\omega}(\mathbf{r}, \mathbf{r_i}), d\mathbf{r_i}, \qquad (2)$$

where

$$G_{0,\omega}(\mathbf{r_a}, \mathbf{r_b}) = \frac{i}{4c_0^2} H_0^{(1)}(k|\mathbf{r_a} - \mathbf{r_b}|) \qquad (3)$$

is the Green's function in a free space environment without flow for a harmonic source of pulsation ω at position $\mathbf{r_a}$ emitting at position $\mathbf{r_b}$ and $G_{0,\omega}^*$ its conjugate, $H_0^{(1)}$ is the *Hankel function* of order 0, k is the wavenumber. The vector $\mathbf{r_i}$ refers to the position of each transducer, $\mathbf{r_0}$ is the source initial position and "*TRM*" denotes an integration over the mirror extent.
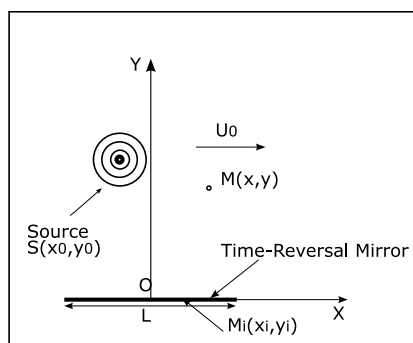

Figure 2: *Monopolar source and TRM in a uniform flow: rectangular and polar coordinates*

Medium in a uniform flow

Here, a stationary uniform one-dimensional flow $\mathbf{u_0}$ parallel to the the array is added to the free space environment. To perform the phase conjugation, this flow has to be reversed. Thus the pressure field is given by:

$$P_{pc}(\mathbf{r}, \omega) = \int_{TRM} G_{u,\omega}^*(\mathbf{r_i}, \mathbf{r_0}) G_{-u,\omega}(\mathbf{r_i}, \mathbf{r_0}), d\mathbf{r_i}, \qquad (4)$$

where $G_{u,\omega}(\mathbf{r_a}, \mathbf{r_b})$ is the Green's function in a free space environment with a uniform flow $\mathbf{u_0}$ parallel to the TRM for a harmonic source of pulsation ω at position $\mathbf{r_a}$ emitting at position $\mathbf{r_b}$. In rectangular coordinates (as shown in Figure 2), $G_{u,\omega}$ is given by [5]:

$$
\begin{aligned}
G_{u,\omega} = {} & \frac{i}{4c_0^2} \cdot \frac{\exp\left(ik\frac{M}{1-M^2}(x_i - x_0)\right)}{\sqrt{1 - M^2}} \\
& \times H_0^{(1)}\left(\frac{k\sqrt{(x_i - x_0)^2 + (y_i - y_0)^2(1 - M^2)}}{1 - M^2}\right)
\end{aligned}
\qquad (5)
$$

where M is the Mach number defined by $M = |\mathbf{u_0}|/c_0$. The coordinates (x_0, y_0) refers to the source position, (x_i, y_i) corresponds to the transducers position and (x, y) refers to an observation point. The Green's function $G_{-u,\omega}$ related to the reversed flow is obtained by replacing M by $-M$ in (5).

2.3 Spatial resolution

One of the main difficulties in detection and imaging methods (beamforming, microscopy, holography, photography, etc.) is the separation of two close objects. Indeed, for an imaging device, the image of a point-like object is not really a point but a spot (often called *focal spot*) resulting from diffraction effects. Thus it is obvious that the larger is the spot, the more difficult is the separation of two point-like objects. The spatial resolution is defined as the required minimal distance between two objects to detect them separately. The commonly used criteria is the *Rayleigh's criteria* : the peak of the first focal spot peak must fall on the first zero of the second focal spot. Quantitatively, if A is the maximum magnitude of the focal spot, the resolution is the spot width at $\frac{A}{\sqrt{2}}$.
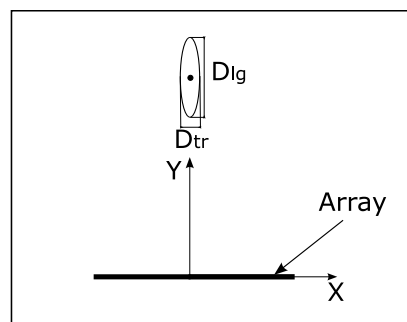

Figure 3: *Focal spot with a TRM : transverse resolution (D_{tr}) and longitudinal resolution (D_{lg})*

The spatial resolution notion can then be introduced in time-reversal. In the case of a closed cavity, the resolution is limited only by the wavelength [7]. The diffraction is caused by the superimposition of the converging and the diverging waves during the time-reversal. In the case of a time-reversal mirror, the focal spot width is linked to the array specifications (length, distance between each transducers), the array-source distance and the wavelength. It is important to note that there is a privileged direction since the array is one-dimensional. Two spatial resolutions can then be defined for a focal spot : the transverse resolution (along the array) and the longitudinal resolution (perpendicular to the array).

Mathematical formulas exist to calculate the spatial resolutions from the above-cited parameters. In far-field ($R > kL^2/2$), Kim *et al.* suggest the following expression for the

transverse resolution [1] in the case of a source in the central axis:

$$D_{tr} = 0.886\lambda.\frac{R}{L}, \qquad (6)$$

where R is the distance between the array and the maximum of the focal spot. He also proposes a mathematical expression (in the case of a source in the central axis) for the longitudinal resolution, considering the phase difference from the focal spot center:

$$D_{lg} = 6\lambda\left(\frac{R}{L}\right)^2. \qquad (7)$$

Finally, a one-dimensional linear array can introduce localization errors, particularly in the normal direction (see section 4.1). That is why the spatial resolution must be calculated at the position of focal spot maximum, which can be more or less different from the real source position.

In the next section, time-reversal numerical simulations with a harmonic monopolar source in a uniform flow and a linear array are described. The results in terms of resolution and localization errors are compared to the theory and discussed.

3 Numerical model for time-reversal in flows

Propagation of waves can be simulated by solving the *Linearized Euler Equations* (EEL) [5] obtained from the conservation of mass, momentum and energy. Then each quantity (pressure, density and velocity) is split into mean and fluctuating quantities, denoted respectively by the subscript $(.)_0$ and the symbol $(.)'$. Finally, the EEL are obtained by writing the conservation equations at the first order:

$$\frac{\partial \mathbf{U}}{\partial t} + \frac{\partial \mathbf{E}}{\partial x} + \frac{\partial \mathbf{F}}{\partial y} + \mathbf{H} = \mathbf{S}, \qquad (8)$$

where :

$$\mathbf{U} = \begin{pmatrix} \rho' \\ \rho_0 u' \\ \rho_0 v' \\ p' \end{pmatrix}, \quad \mathbf{E} = \begin{pmatrix} \rho_0 u' + \rho' u_0 \\ \rho_0 u' u_0 + p' \\ \rho_0 u_0 v' \\ p' u_0 + \gamma p_0 u' \end{pmatrix}, \qquad (9)$$

$$\mathbf{F} = \begin{pmatrix} \rho_0 v' + \rho' v_0 \\ \rho_0 u' v_0 \\ \rho_0 v_0 v' + p' \\ p' v_0 + \gamma p_0 v' \end{pmatrix}. \qquad (10)$$

The vector $\mathbf{U}$ contains the three main quantities (density, pressure and velocity), $\mathbf{E}$ and $\mathbf{F}$ are the *fluxes terms*, $\mathbf{S}$ is the *source term*. Finally, $\mathbf{H}$ contains the mean flow gradients and its expression is specified in reference [5]. The time-reversal is then done by replacing the time variable t by $T - t$ (T is added to ensure the causality) and the velocity components (u, v) by $(-u, -v)$.

A series of time-reversal simulations have been performed with a known source in a two-dimensional space. The propagation in a free-space environment was carried out by solving the Linearized Euler Equations. Spatial derivatives were calculated with a dispersion-relation-preserving finite difference scheme (order 4) [4] and time derivatives were computed with a Runge-Kutta scheme of order 4. The main simulation parameters are presented in table 1. Two sizes of domain

Domain size	200 x 310, 200 x 500
Δx	1
Δy	1
CFL	0.75
Δt	0.75
Source magnitude	0.5
Source wavelength	10
Mach number	[0,0.1,0.2,0.3,0.4,0.5]
Number of iterations	[940,1280]

Table 1: *Time-reversal simulation parameters*

were used, depending on the array-source distance. In all figures, spatial resolution and distances are nondimensionalized according to wavelength λ. The general procedure for carrying out the time-reversal simulation is detailed in references [9, 11].

4 Results

Here, numerical and theoretical results concerning the error of localization and the spatial resolution are compared and investigated. Theoretical results are obtained by computing the integrals (2) or (4) with the Simpson's method. For all simulations, the source is on the central axis of the TRM.

4.1 Localization error

A time-reversal mirror does not surround the source to be located. Thus, there is an inherent lack of information in the normal direction, as pointed out in the previous section. As a result, some errors in terms of localization can appear in some configurations, according to the array-source distance and the length of the array. In this section, the source is on the array central axis so that the localization error is only along the y-axis. The distribution of the root mean square of the pressure obtained from the time-reversed is computed. The source position is then estimated by searching for the maximum of this distribution (within the focal spot). The distance R between the array and the maximum of the focal spot is called distance of focalization. The array-source distance is noted R_0.

Figure (4) shows a distribution of acoustic pressure root mean square obtained by time-reversal along x and y-axis. The source is at position $(0, 0)$ and the ratios R_0/λ and L/λ are set to 15.5. Figure (4b) shows that the localization error does not exceed one wavelength.

Figure (5) shows the evolution of the localization error ε_y along y-axis as a function of R_0/L for a Mach number equal to 0, 0.1, 0.3 and 0.5. Theoretical and numerical results are very close, which validates the numerical approach. For R_0/L ratios greater than 1, ε_y increase almost linearly. As a result, for a proper localization of the source, L must not exceed $1.5R_0$. It is also interesting to note that the error localization decreases with the flow velocity (which is parallel to the array).

4.2 Spatial resolution

Here, some results about spatial resolution with and without flow are presented and discussed. The numerical results
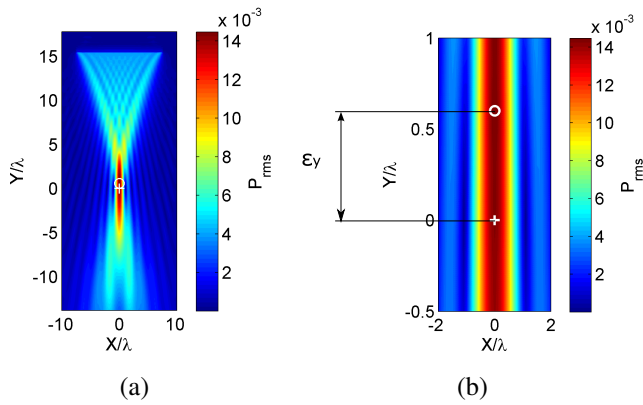
(a) (b)

Figure 4: *Distribution of acoustic pressure root mean square obtained by time-reversal, $R_0 = L = 15.5\lambda$. The cross indicates the source position, the circle corresponds to the peak of the pressure field and ϵ_y is the localization error along y-axis. (a) Global view and (b) magnification.*
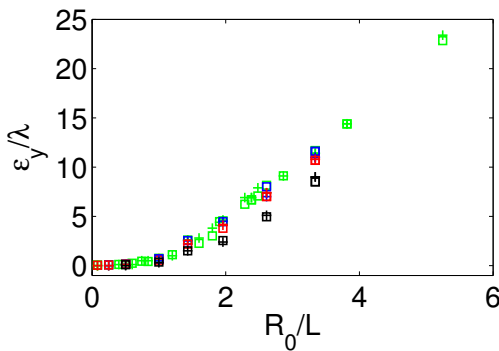

Figure 5: *Localization error ε_y/λ along the y-axis as a function of the array-source-distance-array-length ratio. The crosses correspond to the theoretical results and the squares correspond to the simulation results. In green, the Mach number M is equal to 0, in blue, $M = 0.1$, in red, $M = 0.3$ and in black, $M = 0.5$.*

are obtained from the profiles of the normalized root mean square of the pressure and the theoretical results are obtained from the normalized profiles of pressure Fourier transform by computing integrals (2) and (4).

Medium at rest

Figure(6) shows the pressure profiles along x-axis and y-axis at the pressure field peak. The source is at position $(0, 0)$. The ratios R_0/λ and L/λ are equal to 15.5. As the array has a finite aperture, side lobes due to diffraction appear besides the main lobe. One can note that only the x-profile is symmetrical. Numerical and theoretical results give exactly the same main lobe width (thus the same resolution) and the same number of grating lobes. These profiles are used to measure the transverse and longitudinal resolutions. Figure 7 present the theoretical and numerical results for transverse and longitudinal resolutions. The array length is fixed at $L = 15.5\lambda$ and the results are plotted as a function of the focalization distance. Again, the simulations results are very close to those obtained from Eq. (2). Moreover, concerning the transverse resolution, although simulations have not been carried out in the far-field conditions suggested in [1], the ap-
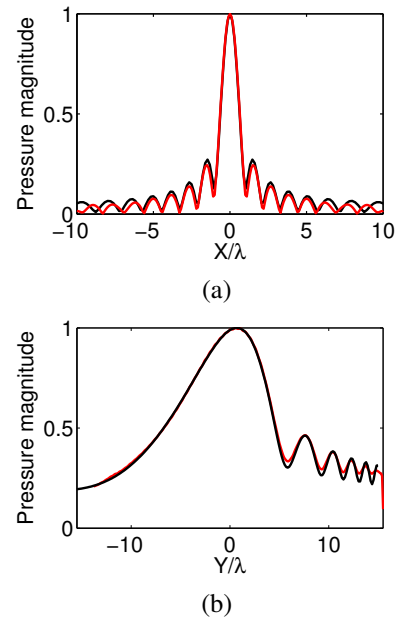

(a)

(b)

Figure 6: *Medium at rest: pressure profiles at the field peak along (a) x-axis and (b) y-axis for $R_0/\lambda = L/\lambda = 15.5$. The black curve corresponds to the theoretical profile and the red curve corresponds to the simulation results.*
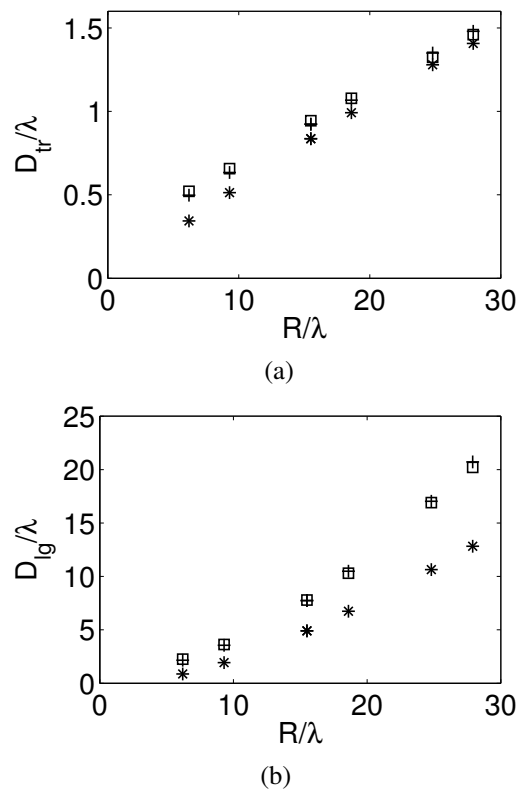

(a)

(b)

Figure 7: *Medium at rest: (a) transverse resolution and (b) longitudinal resolution as functions of focalization distance r for $L/\lambda = 15.5$. (+) theoretical results obtained with Eq. (2), ($\square$) simulations results, ($*$) resolutions obtained with Eq. (6) and Eq. (7), respectively for (a) and*

proximated formula (6) does not differ from more than $\lambda/2$ from the exact calculation. Conversely, the mathematical expression of the Eq. (7) for the longitudinal resolution leads to an error that can reach 50% of the exact calculation. Finally, one can notice that longitudinal focal spot width increases

more rapidly, which is explained by the one-dimensional geometry of the array.

Medium in a uniform flow

A series of simulations has bee run with a one-dimensional uniform flow parallel to the array for Mach numbers $0.1 \leq \mathcal{M} \leq 0.5$. The source is at position $(0,0)$. Effects of this configuration on spatial resolution are investigated. Figure
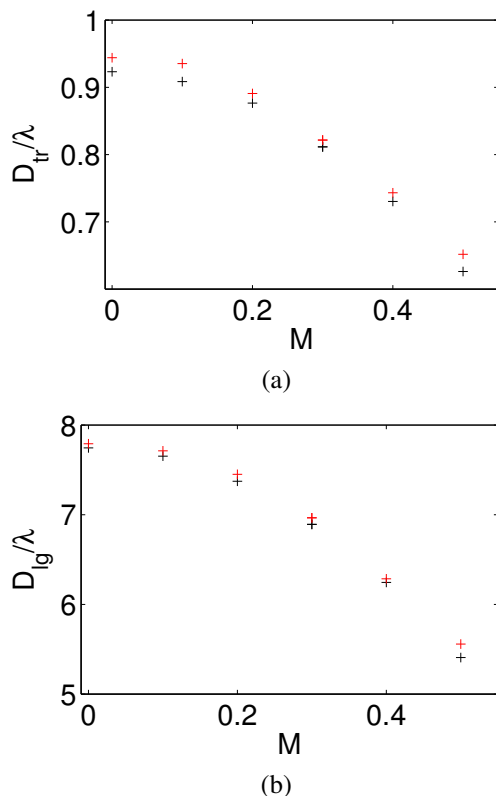

(a)

(b)

Figure 8: *Medium in a uniform flow: (a) transverse resolution and (b) longitudinal resolution as functions of the Mach number for $R_0/\lambda = L/\lambda = 15.5$. Black crosses refers to theoretical results and red crosses correspond to simulations results.*

8 shows the evolution of transverse and longitudinal resolutions as a function of the Mach number (Figure 2). The theoretical and numerical results are very close and show that transverse and longitudinal focal spot widths decrease with the flow velocity. The improvement in resolution from $\mathcal{M} = 0$ to $\mathcal{M} = 0.5$ is about 30%. The increase in the Mach number probably results in an increase of the effective aperture of the array, improving the resolution of the localization.

5 Conclusion

In this study, time-reversal simulations have been achieved with and without flow for a monopolar harmonic source recorded by a Time-Reversal Mirror. The transverse and longitudinal resolutions have been measured and compared to models given by phase-conjugation theory and gives very close results. In a medium at rest, transverse resolution increases linearly according the focalization distance and is close to the far-field approximation given by S. Kim *et al.*. Longitudinal resolution increases in a parabolic way, as predicted by Eq. (7). To keep a localization error perpendicular to

the TRM lower than one wavelength, the array-source distance must not exceed the array length. Moreover, acceptable transverse and longitudinal resolutions are obtained for ratios $R_0/\lambda \leq 15.5$. The effect of a flow parallel to the array has then been investigated. It has been observed that the longitudinal and transverse resolution tend to decrease when the flow Mach number increases, which is probably the result of an increase of the effective aperture of the array.

References

[1] S. Kim, G.F. Edelmann, W. A. Kuperman, W. S. Hodgkiss, H. C. Song, "Spatial resolution of time-reversal arrays in shallow water", *J. Acoust. Soc. Am.* **110** (2), 820-829 (2001)

[2] Darrell. R. Jackson, D. R. Dowling, "Phase conjugation in underwater acoustics", *J. Acoust. Soc. Am.* **89** (1), 171-181 (1991)

[3] D. R. Dowling "Phase-conjugate array focusing in a moving medium" *J. Acoust. Soc. Am.* **94** (3), 1716-1718 (1991)

[4] C. K. W. Tam, J. C. Webb, "Dispersion-Relation-Preservation finite difference schemes for computational acoustic", *Journal of Computational Physics* **107**, 262-281 (1993)

[5] C. Bailly, D. Juvé "Numerical solution of acoustic propagation problems using linearized Euler equations", *AIAA Journal* **38** (1) 22-29 (2000)

[6] Didier Cassereau, Mathias Fink "Time reversal of ultrasonic fields - Part III : Theory of the closed time-reversal cavity", *IEEE* **39** (5) 579-592 (1992)

[7] M. Fink, D. Cassereau, A. Derode, C. Prada, P. Roux, M. Tanter, "Time-reversed acoustics", *Rep. Prog. Phys.* **63** 1933-1995 (2000)

[8] E. Bavu, C. Besnainou, V. Gibiat, J. de Rosny, M. Fink, "Subwavelength sound focusing using a Time-Reversal acoustic sink", *Acta Acustica united with Acustica* **93** 706-715 (2007)

[9] Thomas Padois, "Localisation de source acoustique en soufflerie anéchoïque par deux techniques d'antennerie: formation de voies et retournement temporel numérique", Ph. D. thesis, University of Poitiers (2011)

[10] J. J. Christensen, J. Hald, "Technical review - Beamforming" *Bruël & Kjær* **1** (2004)

[11] T. Padois, V. Graveline, C. Prax, V. Valeau, "Localization of stationary sound sources in flows by using a time-reversal method", *Proceedings of 20th International Congress on Acoustics ICA 2010*, Sydney (23-27 August 2010)

[12] A. Deneuve, P. Druault, R. Machiano, P. Sagaut "A coupled time-reversal/complex differentiation method for aeroacoustic sensivity analysis: towards a source detection procedure", *J. Fluid Mech.* **642** 1-32 (2009)